minerals

MDPI

Article

Airborne Natural Total Field Broadband Electromagnetics—Configurations, Capabilities, and Advantages

Alexander Prikhodko *, Andrei Bagrianski and Petr Kuzmin

Expert Geophysics Limited, Aurora, ON L4G 1G2, Canada
* Correspondence: alexander@expertgeophysics.com

Abstract: The airborne electromagnetic system MobileMT exploits natural fields in a broadband frequency range with offset measurements of magnetic and electric field variations. It was introduced in 2018 and has since been developed in various configurations, each tailored to meet the demands of different exploration tasks, varied terrains, and geoelectrical conditions and support time-domain data with controlled primary field sources. There are four distinct airborne systems: the original MobileMT; the lighter configuration, MobileMTm; the configuration for a drone carrier, MobileMTd; and the innovative time-domain AFMAG hybrid, TargetEM. The paper describes the technical features of each system, their differences and inherent strengths, the optimal usage conditions, and insights into their applications under different conditions across various exploration tasks. Several field case studies are provided to support the natural field electromagnetics capabilities of recovering geological structures in a wide depth range, beginning from the near surface, and address the impact of parasitic IP effects on time-domain data.

Keywords: airborne EM; natural field; mineral exploration; MobileMT

Citation: Prikhodko, A.; Bagrianski, A.; Kuzmin, P. Airborne Natural Total Field Broadband Electromagnetics—Configurations, Capabilities, and Advantages. *Minerals* **2024**, *14*, 704. https://doi.org/10.3390/min14070704

Academic Editors: Marc A. Vallée and Stanisław Mazur

Received: 15 May 2024
Revised: 21 June 2024
Accepted: 10 July 2024
Published: 11 July 2024

1. Introduction

Airborne electromagnetic (EM) systems used in mineral exploration are based on various principles and technical designs, leading to variable performance under different geoelectrical and geological conditions. Systems with controlled primary fields have limitations, particularly in the depth of investigations and the resistivity detectability range (the last in the time-domain method). These limitations are overcome by using "passive" or natural field systems, as confirmed by direct comparisons of "passive" field data (MobileMT) with airborne TDEM data [1]. A brief history of natural field airborne technology development is described by the authors of [2], with a comparison of different systems' technical specifications and their evolution over sixty years. These systems include the original AFMAG used in the 1960s and early 1970s, further experimental prototypes of the AFMAG method (late 1990s–early 2000s), and the magnetovariational tipper-type ZTEM system patented in 2005. The latest development, MobileMT, was introduced to the airborne geophysics market in 2018 [3,4]. It measures natural magnetic (magneto) and electric (telluric) field variations across a wide range of frequencies divided into comparatively narrow windows. Using three orthogonal components to measure magnetic field variations, the system can detect geoelectrical boundaries in any direction, improving subsurface recovery in complex geological structures. The airborne technology is versatile and can be used for various geophysical tasks in diverse geoelectrical and terrain conditions, as well as different survey configurations. Technical adaptations are required for specific conditions, such as using lightweight systems at high altitudes, ensuring precise positioning for detailed surveys, addressing time-domain data insufficiencies, and exploring deeper beneath conductive overburden.

2. Theory and the System Configurations

The operating principle of airborne natural field MobileMT EM technology is a combination of magnetotelluric (MT) and magnetovariational (MV) concepts [2]. The measuring system for all configurations includes two main parts (Figure 1):

- Three orthogonal dB/dT inductive coils (Figure 1b) in a teardrop-shaped shell towed below the helicopter. Variations in the measured magnetic field (H-field) are recorded digitally in an acquisition system placed inside a helicopter. It is unnecessary to monitor or control the tilt precisely because the measurement system provides rotationally invariant total-field data;
- Two pairs of independent grounded orthogonal (X and Y) electric lines (Figure 1a) measure "signal" and "reference" variations in the electric field (E-field). Uncorrelated variations in the E-field, measured separately by the "signal" and "reference" lines, are used to clean the electrical component data [5], assuming the noise is uncorrelated with the signal. This process, using the cross-spectral technique, significantly reduces the risk of biased results [6]. The data from the stationary E-field measurement system are recorded by a separate acquisition system at the same sampling rate as the mobile H-field.

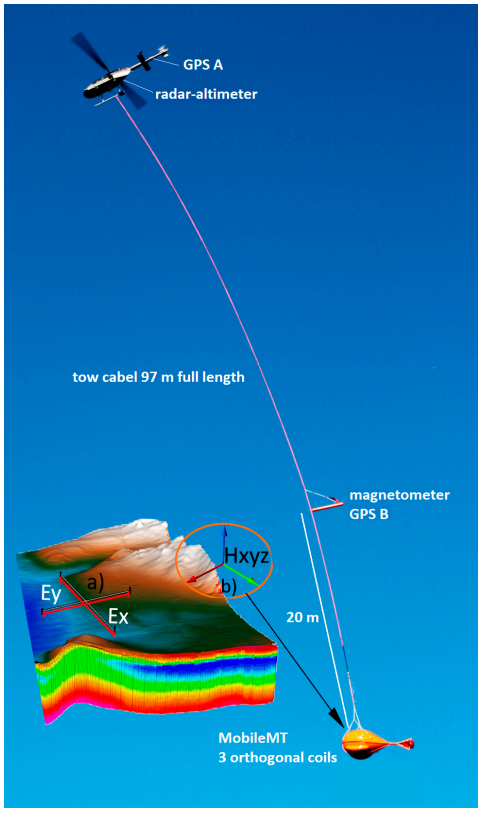

Figure 1. MobileMT system in survey configuration. (**a**) Schematic of a base station that includes two pairs of independent grounded orthogonal electric lines in the same position. (**b**) Schematic of three orthogonal dB/dT inductive coils.

The denoised and corrected E-field data represent the primary natural electromagnetic field variations. They facilitate the separation of the time variance from the space variance of the measured fields (like in MV). The combination of magnetic (H) and electric (E) fields variations are used for the admittance tensor calculation, described by Bostick and Smith [7] as Y = H/E (written in tensor notation) and, ultimately, for the calculation of apparent conductivities corresponding to different frequency bands:

$$\sigma(\omega) = \mu\omega \, | \, Y^2 \, | \, ,$$

where μ is the magnetic permeability of free space, and ω is the angular frequency.

With magnetic and electric field data variations measured in different relative orientations, the magnitudes of the total H and E vectors independent of the sensors' spatial attitudes are calculated at the same frequency and time [5]. The processed data typically span a frequency range of 26–21,000 Hz, divided into 30 windows (Figure 2). The dead-band range, shown as typical in the figure, varies diurnally and seasonally.

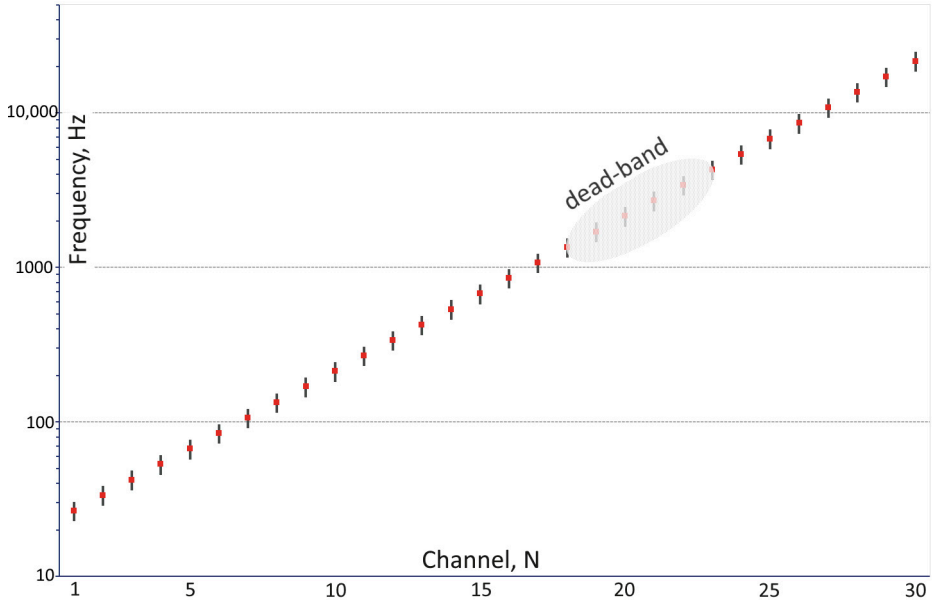

Figure 2. Typical MobileMT data frequency windows with the frequency zone (dead band), where the natural signal strength attenuates to a small level.

Currently, there are four modifications to the MobileMT system, tailored to specific survey requirements or terrain conditions:

(1) The basic model (Figure 1: 1.4 m diameter coils and 97 m tow cable) can provide data in the 26–21,000 Hz bandwidth. The historical lowest acceptable frequency data from the configuration is 22 Hz [5]. The system exhibits minimal mechanical noise, with negligible disturbance from helicopters, and is free from nearby noise sources. A GPS antenna with a Cs magnetic sensor is located 20 m above the magnetic field variations receiver in a separate bird. The system weighs 250 kg;

(2) MobileMTm (Figure 3: 0.7 m diameter receiver coils and 55 m tow cable length). Currently, the recorded frequency range is 50–28,000 Hz. Two Cs magnetic sensors in the horizontal gradiometer configuration (4 m apart), a gyro inclinometer for the magnetic sensors tilt corrections, and a GPS antenna are located on the same frame together with the three components of the magnetic variations receiver. The system weighs 150 kg.

A GPS antenna and a gyro inclinometer on the MobileMTm frame allow accurate retrieval of positions for both the airborne EM sensor and magnetometers. The precise positioning suits detailed surveys with relatively small-line spacing focusing on near-surface targets along the recovering deep structures. In addition, the system's light version (MobileMTm) perfectly matches the surveys' requirements at high altitudes >4000 m above sea level;

(3) The AFMAG component can be derived from streaming data recorded during surveys using the time-domain (TEM) system TargetEM when the MobileMT base station is operational and captures variations in the electric field (Figure 4) [1]. The receiver coils have a diameter of 1 m and are attached to a 50 m long tow cable. In the case of TEM combinations, the extracted natural field frequency range is determined by the base frequency of the controlled primary field source and the current waveform duty

cycle. Typically, the TargetEM system operates at a base frequency of 25/30 Hz, and apparent conductivities are calculated from streaming EM data in the high-frequency range of 5000–28,000 Hz, depending on the natural signal;

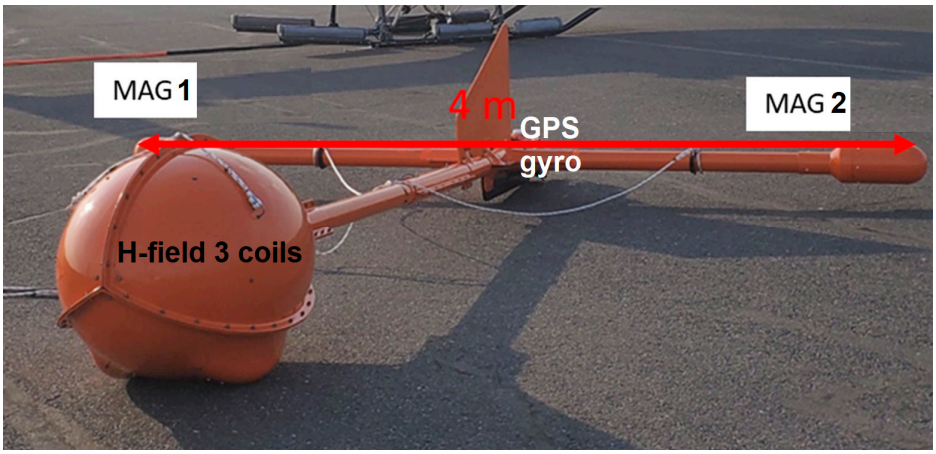

Figure 3. Airborne component of MobileMTm system.

(a) (b)

Figure 4. TargetEM system (**a**), with the ground E-field base station acquisition system (**b**).

(4) MobileMTd is a drone version of the MobileMT system (Figure 5) currently undergoing field tests designed to measure magnetic field variations at lower frequencies of 10-15-20 Hz by mitigating motion noise within this range. These lower frequencies are essential for exploring conductive areas and regions with thick, conductive overburden where the standard 26 Hz system reaches its limits. As illustrated in Figure 6, the system aims to enhance the depth of investigation (DOI), particularly in conducive environments. The DOI typically refers to the sensitivity of acquired data to subsurface petrophysical variations. Spies [8] suggests that the magnetotelluric method can detect a buried halfspace beneath 1.5 skin-depths of overburden. For instance, a 1.5 skin-depth corresponds to 600 m at 5 ohm-m in an infinite halfspace (Figure 6). Moreover, the MobileMTd system offers flexibility in selecting optimal survey times, including during and after sunset, to maximize natural electromagnetic activity peaks.

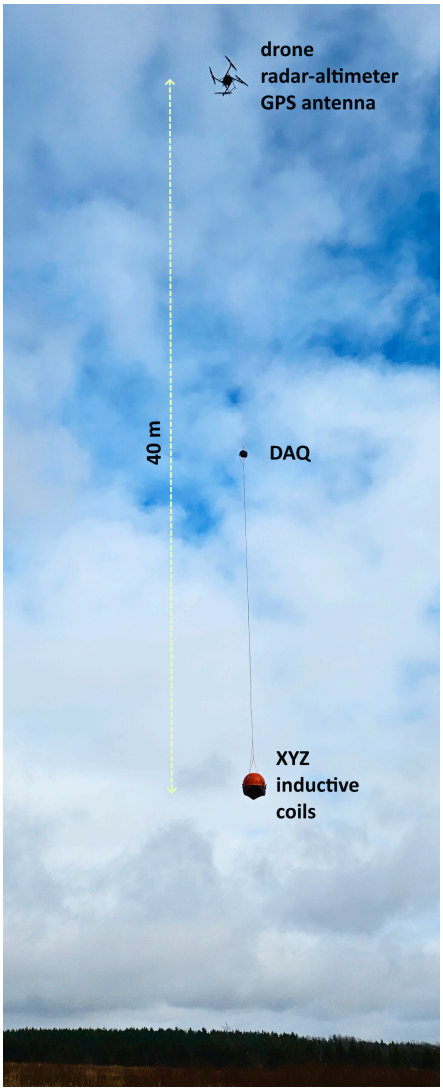

Figure 5. MobileMT system on a drone.

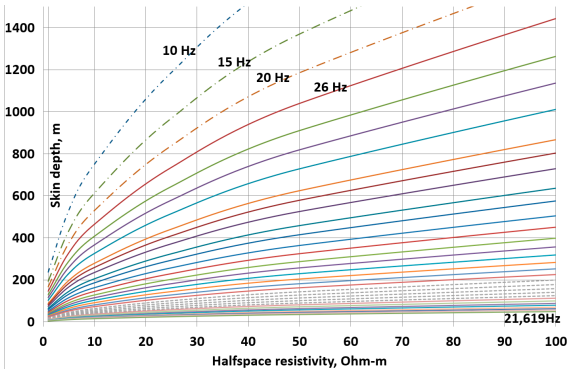

Figure 6. Diagram of 1.5 skin-depth with MobileMTd additional frequencies (10–20 Hz) calculated for conductive halfspace of 1–100 ohm-m.

In addition to natural EM field data, all configurations of MobileMT airborne technology can measure VLF data, extracting the signal from the same magnetovariational streaming data. The VLF total field magnitudes (usually in the 15–30 kHz range) are calculated as a vector of signals from the orthogonal receiver coils.

The natural total field airborne EM system, with its comprehensive technical solutions, effectively explores various types of mineralization across a wide depth range and identifies complex geological settings and structures. Table 1 describes the main technical features of MobileMT technology and their corresponding outcomes.

Table 1. Technical solutions and their outcomes in the system's capabilities.

Technical Solution	Outcome
Primary field: naturally occurring subsurface electromagnetic plane wave.	Depth of investigation consistently exceeds the capabilities of controlled-source airborne EM systems. There is no critical dependence on the system's terrain clearance, as illustrated in [5].
Three orthogonal receiver coils (total field).	Sensitivity to geoelectric boundaries in any direction.
Remote signal-reference electrical component station in the combination of a mobile magnetic component.	Denoised and bias-free data related to the electromagnetic admittance with the calculation of the absolute values of conductivities.
Frequency domain data.	Sensitivity in a full range of rock and mineral resistivity. The method is sensitive to conductors and resistivity differences in the range of thousands and tens of thousands of ohm-m (a proven case up to 20,000 ohm-m [5]).
Broadband frequency range over 3+ decades (typically 26–21,000 Hz).	Imaging of near-surface structures as well as those at >1 km depth, depending on the conductance of the geologic environment.
Output apparent conductivity data for up to 30 different frequencies (typically for 15–24 frequencies, depending on the natural signal).	Better in-depth resolution than ZTEM, with 4–6 frequencies [2] and a good opportunity for data selection, depending on cultural noise sources, natural EM field signal, and exploration goals.

3. MobileMT Capabilities and Advantages on Field Examples

The MobileMT data inversions presented below were executed using the MARE2DEM software code [9] adopted for MobileMT data. The data inversions were executed without constraints using a uniform halfspace as an initial model.

3.1. Athabasca Basin (Canada): Comparison with Natural Field Airborne System ZTEM (Tipper Data) and Ground TAMT

Athabasca Basin has historically presented a challenging environment for testing geophysical technologies, including airborne electromagnetic (EM) systems. This unique geological region offers a practical testing ground for several critical parameters: depth of investigation, resistivity resolution (including in high-resistivity bands), sensitivity to different boundary orientations, and the ability to recover complex structures and a low-contrasting contact.

The study area is located in the western part of the Athabasca Basin (Figure 7). The known unconformity-type uranium deposits (Collete, 58B, Kianna, Anne) are controlled by the NNW trending, graphite-rich "Saskatoon Lake Conductor (SLC)" [10]. The Athabasca Group sandstone with thickness between 710 m and 750 m unconformably overlies basement crystalline rocks and granitic and pelitic gneisses [11]. There are three types of uranium mineralization displayed on the Kianna deposit: unconformity mineralization associated with the conductive graphitic fault (SLC) and followed by intense chlorite–pyrite alteration; basement mineralization in steep-to-moderate dipping veins with intense clay–chlorite alteration; and above the unconformity alteration plume containing perched mineralization, followed by clay–chlorite alteration. The last "often occurs along the up-dip projection of basement-hosted faults into the sandstone column" [10].

The MobileMT system was tested in 2018 over the Shea Creek uranium deposit along a line and compared with the ZTEM system testing results [12] (Figure 7). The ZTEM system, a predecessor of MobileMT technology, measures only one vertical component of the magnetic field (Hz) along survey lines [2]. The orthogonal horizontal components of the magnetic field Hx and Hy are measured at a remote, stationary base station to reference the primary field variations. In contrast to MobileMT, ZTEM does not utilize the

data acquired at the station as a reference to denoise the data, which could cause biased tipper data [13]. Other limitations of the tipper-type system include a lack of ability to image layered geology [13], a reduced bandwidth, a limited number of frequencies, and comparatively wide frequency windows [2].

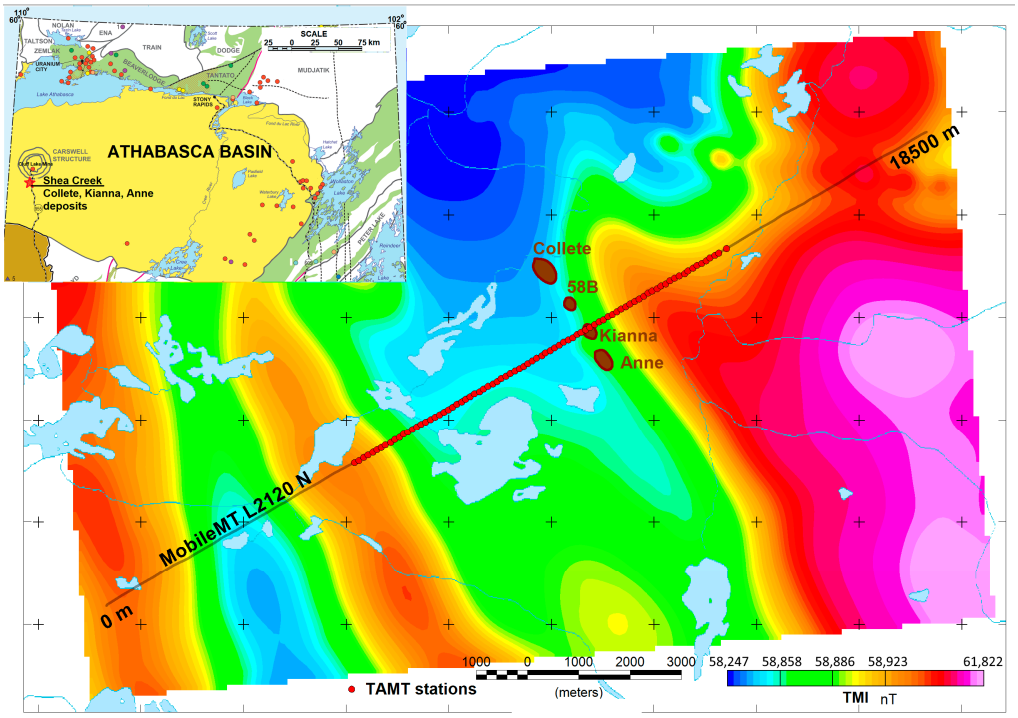

Figure 7. MobileMT (and ZTEM [12]) survey line with positions of TAMT stations on a magnetic field map of the study area. The overview geological map from the Mineral Resource Map of Saskatchewan, 2008 edition (Saskatchewan Ministry of Energy and Resources). Magnetic field data and the overlapped hydrology from Canada Geoscience Data (http://gdrdap.agg.nrcan.gc.ca, accessed on 6 May 2024).

Figure 8 compares resistivity sections derived from MobileMT and ZTEM data along the same survey line crossing the SLC with the Kianna deposit [10] and the Klarke Lake structural conductor. Apparent conductivities across twelve frequency windows used in MobileMT data inversions are displayed in the resistivity section. While both systems detect major conductive structures, they differ in performance in several aspects. Unlike ZTEM, the MobileMT system clearly identifies the unconformity contact between the more resistive Athabasca sandstones and basement rocks at a depth of 700–750 m below the surface. On the right side of the survey line, ZTEM depicts a continuous conductive layer at the top, ranging from 700 to over 1000 m thick, interpreted as Douglas Formation mudstones [12]. According to the descriptions of stratigraphy and sedimentology of the western Athabasca Basin, the thickness of Douglas Formation mudstones typically does not exceed 200 m [14]. MobileMT provides a more detailed depiction in this segment, revealing a near-surface conductive layer with a thickness of approximately 200 m (likely corresponding to the Douglas Formation mudstones) and a distinct conductor in the basement.

Data from the ground transient audio magnetotellurics (TAMT) method exploiting linearly polarized signal of sferics [15] were collected in the summer of 2005 over the Shea Creek deposit [16]. One of the ground survey lines crosses the Kianna mineralization zone and lies in the central part of the MobileMT and ZTEM test line, as shown in Figure 7. The TAMT resistivity section extracted from a 3D model of the tipper data is shown in Figure 9, along with MobileMT resistivity distribution in the same line range. The shape of the Saskatoon Lake conductor, as recovered from MobileMT data, is well-aligned with the results of the ground TAMT survey (Figure 9).

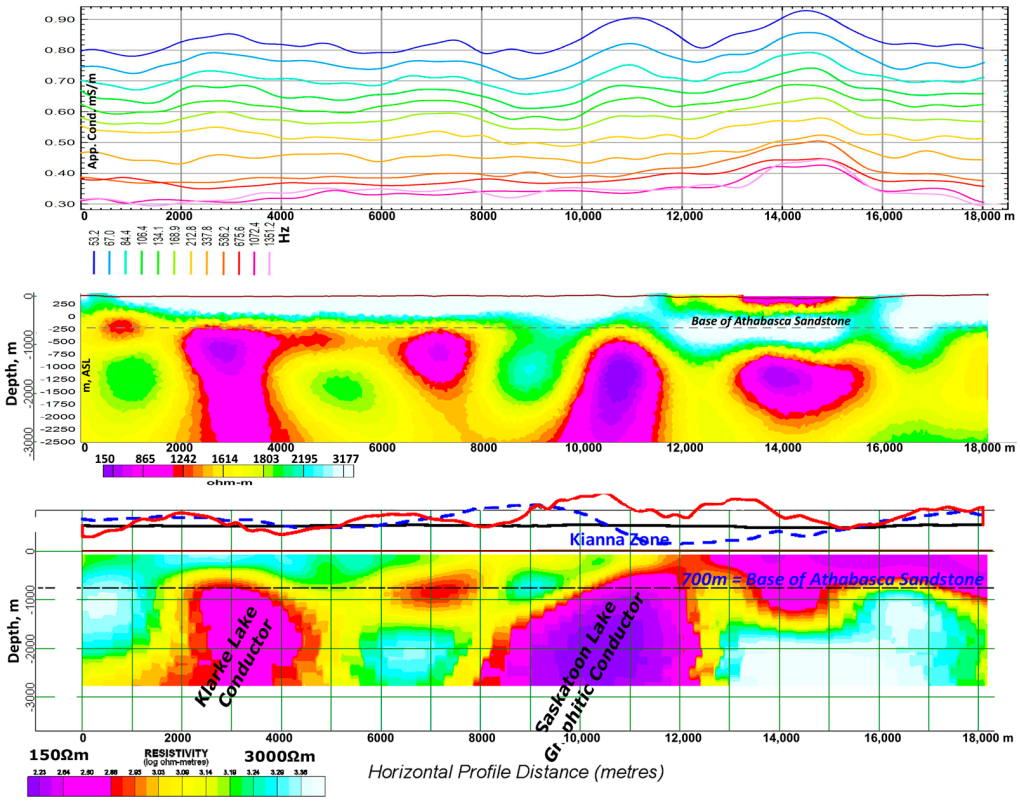

Figure 8. MobileMT apparent conductivity profiles (**top**); MobileMT resistivity section (**middle**) and ZTEM resistivity section (from [12], **bottom**) over the line crossing Kianna uranium mineralization zone.

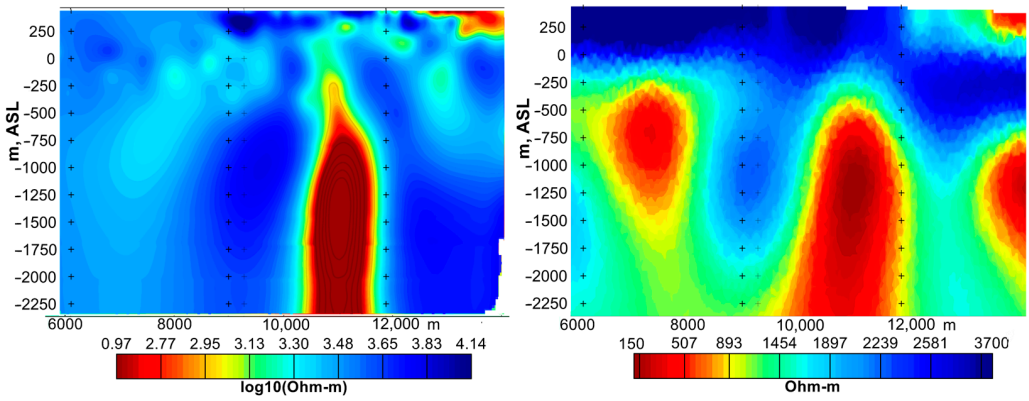

Figure 9. Kianna zone: **left**—resistivity section extracted from ground TAMT tipper (Zxy/Zyx/Tx/Ty) 3D model; **right**—MobileMT resistivity section.

3.2. VMS Mineralization System El Domo (Ecuador)

The El Domo deposit is a gold-rich, polymetallic VMS deposit located in the Western Cordillera of Ecuador. The mineralization is flat-lying, stratiform, and stratabound and occurs in one main massive sulfide lens, a directly overlying talus or breccia zone, and a number of smaller, mineralized lenses, primarily in the footwall of the main lens [17,18]. The lens thickness ranges between 20 cm and 25 m and strictly follows the contact between the Lower Felsic Unit and the Hangingwall Unit (Figure 10). Sphalerite, chalcopyrite, and pyrite are the principal sulfides in the mineralized rocks. Galena is less common, and tennantite/tetrahedrite and covellite are minor phases. The known lateral dimensions of the VMS massive sulfide mineralization are approximately 1,000x800 m. The massive sulfides are related to a zone of abundant hydrothermal alteration, which includes extensive sericitization–silicification in the rhyodacitic footwall and widespread

silicification–chloritization–argillitization in the overlying mafic volcaniclastic rocks. The rhyodacite hosts a sulphide-rich stockwork zone and abundant gypsum, replacing earlier anhydrite. The stockwork is characterized by quartz–sericite alteration and includes massive pyrite mineralization, which is irregularly replaced by abundant chalcopyrite [17]. The El Domo model type showcases distinct zoning, starting from the underlying feeder pipe area (considered the stockwork) and extending through vertical and lateral variations up to the abrupt termination of the massive sulfides [17].

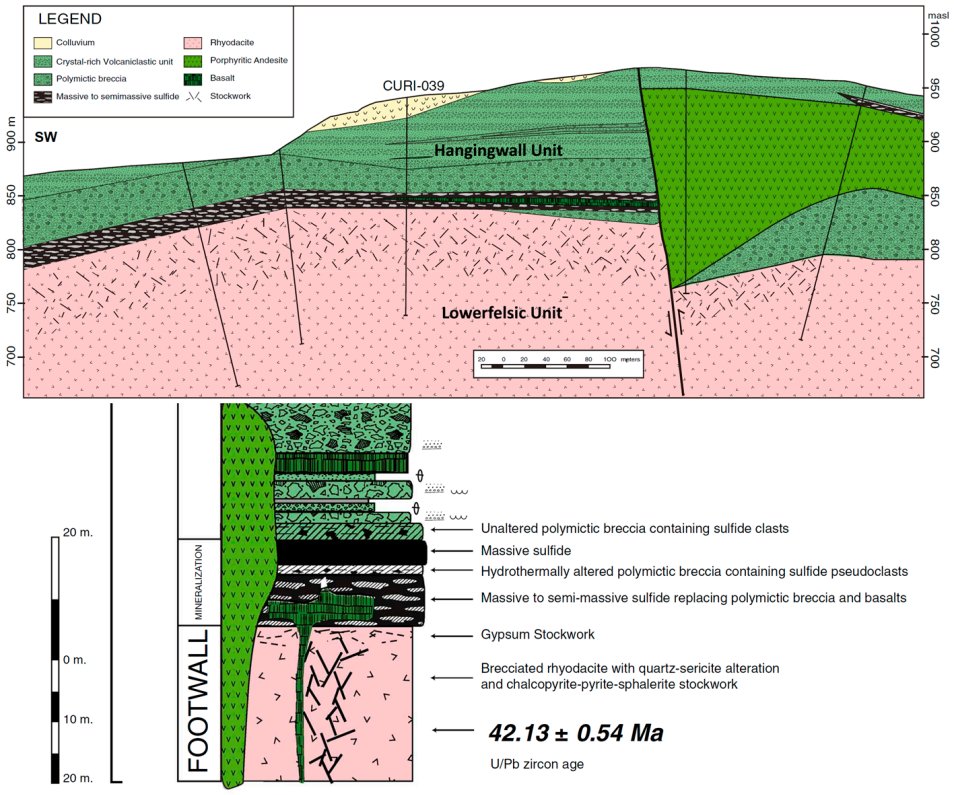

Figure 10. Geological section (**top**) and stratigraphic column (**bottom**) of El Domo deposit [18].

There is no proven evidence from historical geophysical data that the main lens of El Domo VMS mineralization is conductive compared to the surrounding rocks. If sphalerite, a non-conductive mineral, is the primary mineral in the massive sulfides assemblage, while pyrite and chalcopyrite are found disseminated or aggregated with quartz and barite, as indicated in [17], then the lens' potential for high conductivity is questionable. The MobileMT survey results suggest that the flat-lying mineralization is located on the contact between the resistive rocks of the Hangingwall Unit and the conductive footwall (Figure 11), as the drilling results indicate directly [17,18]. The conductive zone exhibits complex structure boundaries, likely indicating alteration zones associated with the stockwork controlling VMS mineralization as a feeder structure rather than uniformly representing Lowerfelsic Unit rocks. Figure 12 shows the resistivity distribution around the El Dome deposit in a 3D view. The El Domo case study demonstrates MobileMT's capabilities in recovering comparatively near-surface geology and deep structures, including complex geometry.

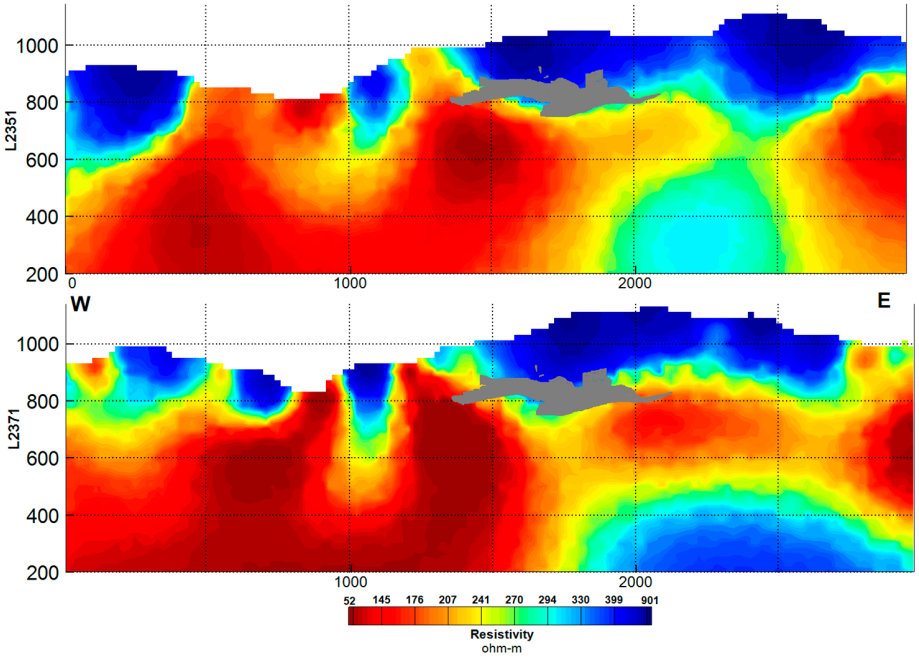

Figure 11. MobileMT resistivity sections along survey lines crossing El Domo deposit (distance between L2371 and L2351 lines is 200 m). Grey—projection of stratabound VMS mineralization on the survey lines.

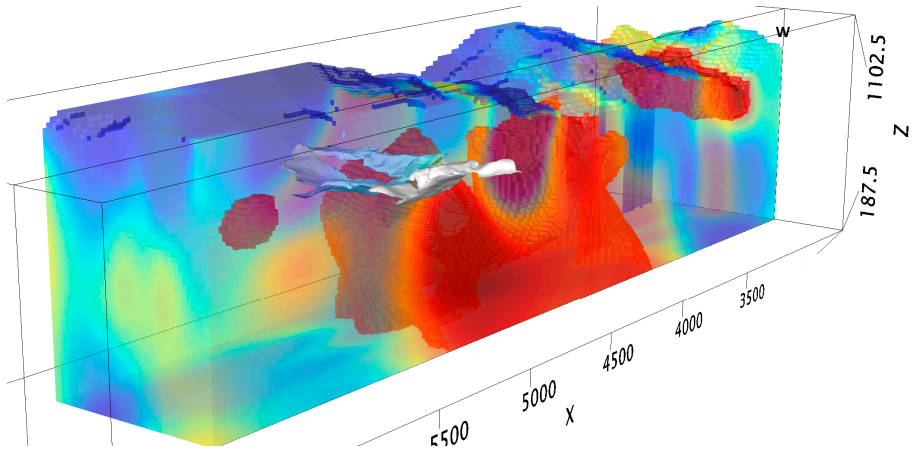

Figure 12. MobileMT resistivity 3D voxel with the El Domo VMS mineralization position (grey).

3.3. Sudbury Impact Structure (Canada)

One of the main environments of the Ni-Cu sulfide and platinum group element (PGE) mineralizations in the 1.85 Ga Sudbury impact structure is the near basal contact and the underlying anatectic footwall breccia [19]. The contact of the Sudbury Igneous Complex (SIC) contains a significant amount of pyrrhotite with pentlandite and chalcopyrite, but the PGE mineralization at Sudbury is not always associated within the highest concentrations of sulfide and often occurs hundreds of meters away from the Ni–Cu mineralization and within the footwall rocks [20]. The SIC footwall strata, associated breccia, and their inflections and hanging forms are important structural and lithological factors in controlling both types of mineralization in the geological structure.

Moderately conductive bodies within the norite, contact sublayer, and footwall breccia area were mapped using heliborne frequency-domain data employing coplanar (32,000 and 4175 Hz) and coaxial (4600 and 935 Hz) coil pairs [21]. Both MobileMT airborne EM technology and the frequency-domain method can detect not only highly conductive sulfide concentrations but also moderately and low-conductive structures and lithologies [2].

MobileMT operates across a broader spectrum of frequencies, enhancing its depth of investigation (DOI) compared to frequency-domain systems with controlled primary field sources. MobileMT's DOI is estimated to reach nearly 2 km in the Sudbury resistive environment. The lowest frequency used in MobileMT data inversions was 84 Hz due to interference from nearby powerlines and industrial sources affecting lower frequencies. The results from MobileMT EM data inversion along a test line crossing the SIC contact in its southwest end are presented in Figure 13, demonstrating a depth of investigation estimated to exceed 2000 m, based on a sensitivity measure of approximately −2.7 on a log10 scale (Figure 14).

The position of the line is shown on the geological map (Figure 15). The conductive footwall between the SIC and Precambrian igneous rocks has been mapped successfully. The test survey results demonstrate MobileMT's capability of detecting and recovering deep structures, which are not reachable by conventional airborne EM systems with towed controlled sources of the primary field.

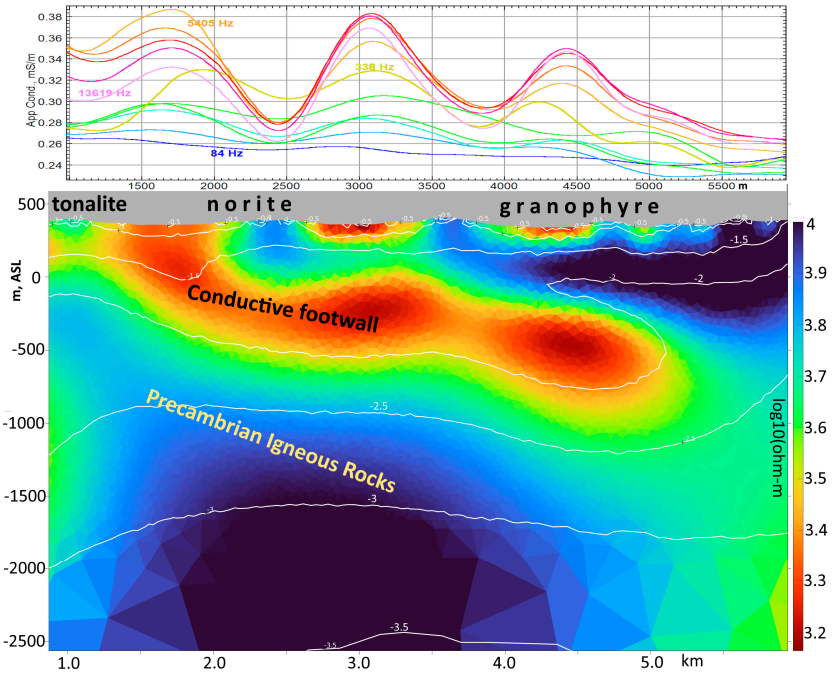

Figure 13. MobileMT apparent conductivity profiles in 84–13,619 Hz bandwidth (**top**) and resistivity section with overlapped normalized inversion sensitivity contours (the test survey line position is in Figure 15).

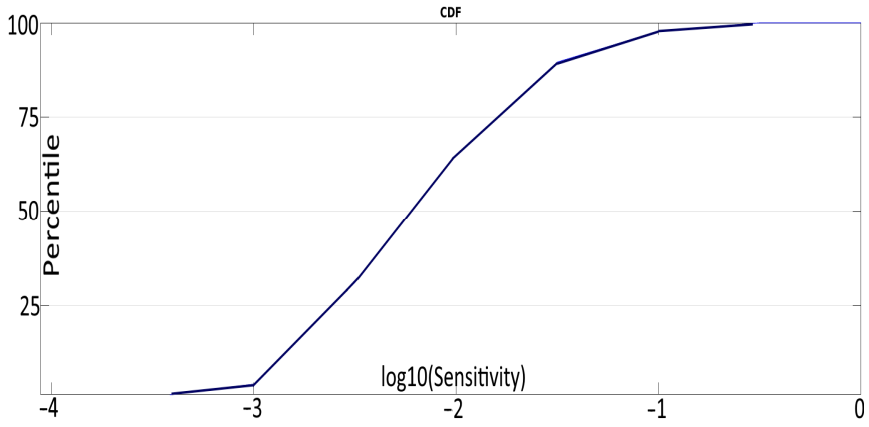

Figure 14. Cumulative distribution function of normalized inversion sensitivity along the survey line in Figure 9.

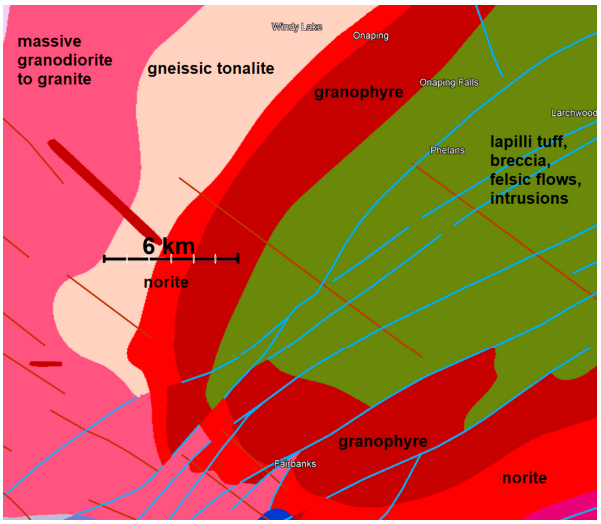

Figure 15. SW of Sudbury impact structure geology (Ontario Geological Survey).

3.4. Poplar Porphyry Deposit (BC, Canada)

Copper–molybdenum porphyry mineralization on the north shore of Tagetochlain Lake is associated with the Late Cretaceous Poplar intrusive stock. The sulfide mineralization occurs within broad envelopes of propylitic, argillic, phyllic, and potassic alteration [22]. Featuring a well-developed pyrite halo, the deposit appears in the MobileMT data as a discrete conductive anomaly that closely matches the deposit boundaries (Figure 16). The Late Cretaceous felsic pluton (Poplar Stock) is distinctly observed as a resistive, dome-like structure in the center of the resistivity sections.

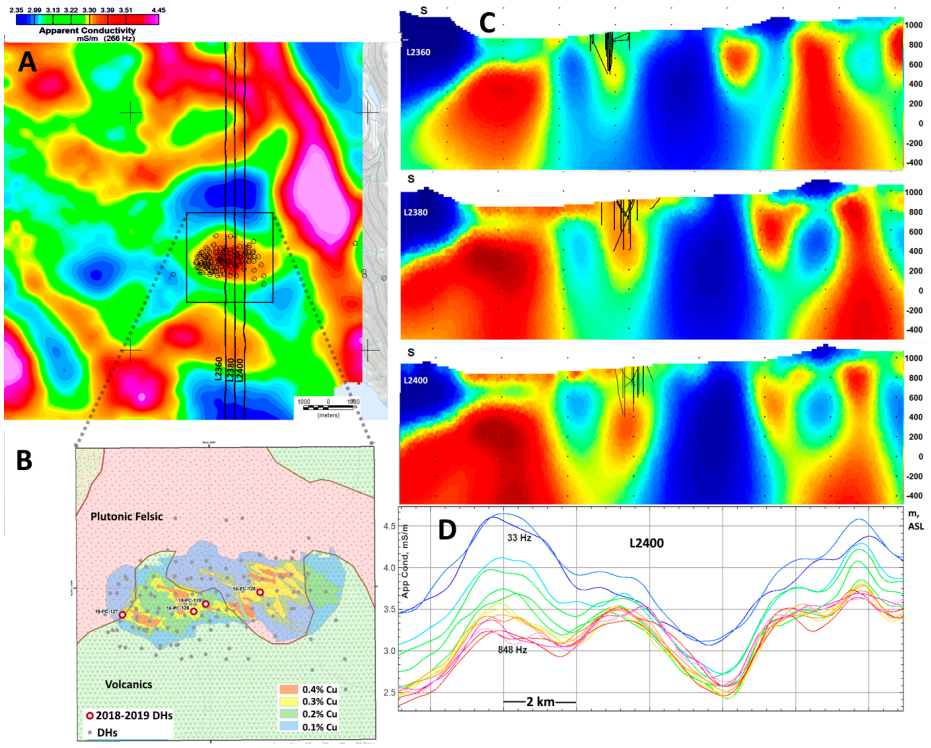

Figure 16. Poplar porphyry deposit: (**A**) Apparent conductivity color grid (266 Hz) with drill hole positions and MobileMT lines crossing the deposit; (**B**) Geological map and Cu grades projected to the surface (from [22]); (**C**) MobileMT resistivity sections along the lines in A, with projections of drill holes; (**D**) MobileMT apparent conductivity profiles along Line 2400.

3.5. Combination with Active Source Time-Domain Data

The TargetEM system was designed to capture both time-domain responses from a controlled-source transmitting field and natural (passive) EM field data [1]. Natural EM field data are recorded between the pulses of the transmitting field and when the transmitter is off as a second option. This combined active and passive airborne electromagnetic system collects broadband streaming data, allowing the extraction of variations in the natural EM field, VLF signals, and time-domain components. Even within a limited frequency range (typically above 5 kHz), natural field data play a crucial role in filling gaps where the time-domain method may be restricted, such as in mapping highly resistive geological terrains, detecting superconductors, conducting surveys in rugged terrain, and identifying parasitic effects, like IP and SPM.

An illustrative field example of TargetEM data comes from Western Australia, specifically within the Norseman-Wiluna Belt of the Kurnalpi Terrane in the Eastern Goldfields Superterrane (EGS). This region is known for significant occurrences of nickel sulfides associated with Archaean greenstone peridotites [23].

TargetEM time-domain data were recorded with a base frequency of 25 Hz and a 420,000 NIA dipole moment, covering 37 time gates within the off-time range of 83.4–12478.30 microseconds. A prominent parasitic IP effect, evident from negative dB/dt responses, significantly influenced induction, particularly in the eastern part of the survey block (Figure 17). Passive EM field and VLF data were extracted from the same streaming data recorded during the survey at a sampling rate of 73,728 Hz. As depicted in Figure 17, discrete conductors were identified within the IP anomaly using complementary high-frequency data extracted between transmitting field pulses.

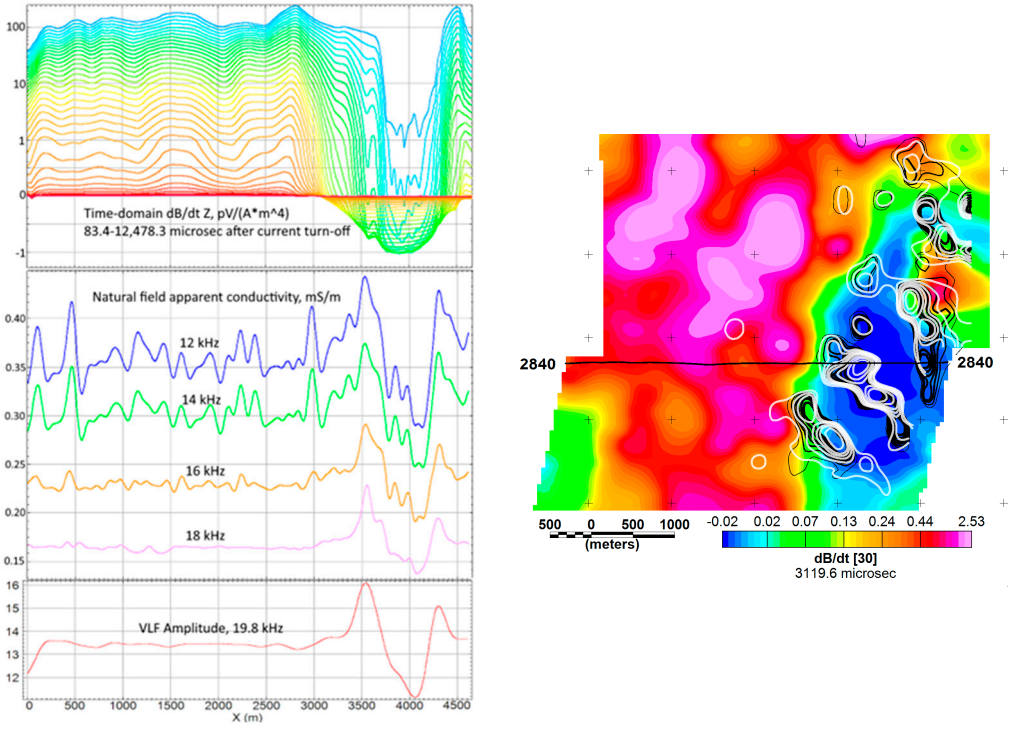

Figure 17. Left: TargetEM time-domain, natural field EM, and VLF data profiles recorded simultaneously along 2840 survey line; right: dB/dt color grid with overlapped anomaly contours apparent conductivity natural field at 18 kHz (white) and VLF at 19.8 kHz (black) (Western Australia).

Furthermore, a comparison between natural field MobileMT data and time-domain data affected by induced polarization due to a superficial clay-rich layer [1] highlights the relative independence (or minimal influence) of MobileMT's natural field data on parasitic effects.

Gasperikova and Morrison [24] demonstrate that natural field (MT) data can be affected by the IP effect only under specific conditions. First of all, the IP component is prominent when telluric (E) field data are measured at a fixed base and along stations during continuous profiling (the TM mode), as E-field data become frequency-dependent in the presence of a polarizable body, indicating the presence of the IP effect. In MobileMT surveys, E-field data are measured only at a stationary position, not over potentially polarized bodies. Favorable conditions to detect the IP influence in natural field data include having a finite polarized body and low frequencies (typically below 1 Hz, outside the MobileMT frequency range), where the body shows negligible induction but still exhibits significant complex frequency-dependent resistivity. Therefore, based on Gasperikova and Morrison's research results and MobileMT survey practices, including measurements over strongly polarized surficial layers [1], MobileMT data are not affected by the IP phenomenon.

4. Discussion

The introduction of MobileMT airborne electromagnetic (EM) technology in 2018 marked a significant advancement in mineral exploration with airborne EM. It leverages natural field measurements to overcome the limitations of traditional controlled-source systems and previously developed natural field systems.

The airborne modification of the magnetotelluric method does not contradict the definition of the method given by Louis Cagniard in 1953, where the measurement of variations in magnetic and electric fields at the same positions (stations) is just a preferable option [2]. The telluric method, which involved the comparison of only horizontal electric fields measured simultaneously at a base-fixed station and remote survey sites, was used from 1939 to 1973 (before and after Cagniard–Tikhonov's discovery) by Schlumberger, Berdichevskiy, and Yungul [25]. The fundamental point of Cagniard–Tikhonov's discovery is the canceling of variations from far-zone natural sources in measured data by the mutual normalization of telluric and magnetic field components [26], and this principle is at the core of MobileMT technology. In the ground telluric–magnetotelluric method, the telluric transfer tensor (T) between the electric fields measured at different stations (r and b) is expressed as $E^r = [T]*E^b$ [25], and similarly, the magnetotelluric tensor in MobileMT is expressed as $H^r = [T]*E^b$ [5]. Combining the offset E-field and H-field in the resulting output data, as well as the total field measurements, requires modifying the standard inversion codes, as noted in [13], and several consulting groups have already achieved this. The 3D inversion of MobileMT data is implemented in EMvision (TecnoImaging), E3dMT (UBC-GIF), GeoTools (Viridien), and MAGNUM (Geotexera) software, to name a few examples.

Airborne natural field technology has several advantages over ground methods. The advantages include high-density coverage of comparatively large territories in a reasonable time, encompassing high-altitude regions, mountainous landscapes, deserts, and other hard-to-reach areas. Additionally, there are significant economic advantages. The versatility and depth of investigation offered by MobileMT and its configurations (MobileMTm, MobileMTd, and TargetEM) have enabled the detailed exploration of complex geological environments, even in challenging geoelectrical and terrain conditions. The airborne MT concept has been verified experimentally, as demonstrated in the field examples above and other publications [1–3,5]. The results from these case studies, including direct comparisons with other airborne and ground methods and drilling, highlight the broad applicability of MobileMT technology and its configurations in mineral exploration.

The following implications and future research directions are suggested:

- Enhanced subsurface imaging: MobileMT's ability to measure total natural fields over a broad frequency range allows for deeper penetration and more detailed subsurface imaging in a wide range of resistivities. Future research should focus on refining inversion algorithms and data processing techniques to further enhance the resolution and accuracy of subsurface models;

- Adaptability to diverse environments: The different configurations of MobileMT systems cater to specific survey needs, making them suitable for a wide range of exploration scenarios. Further field tests, particularly with the drone-based MobileMTd, are necessary to validate its performance and extend its applicability in challenging terrains, including very conducive terrains;
- Integration with other electromagnetic methods: Combining MobileMT with other geophysical EM techniques, such as time domain and VLF, extracted from the same streaming data, could provide a more comprehensive understanding of the geoelectrical image of the subsurface from very near-surface to the first kilometers depth. Future research and developments should explore the synergies between these methods to improve integrated exploration strategies with the EM methods in one system;
- Mitigating time-domain and natural field method data limitations: The problematic situations of the airborne time-domain method include the development of parasitic IP and SPM effects, highly resistive geology, and high system altitude in rugged relief conditions. With its comparatively large footprint and broad high-frequency windows, the natural field method has a lower resolution in detecting near-surface features and smaller conductors than the time-domain method. The further development of combined systems that integrate passive- and active-source data will be crucial in overcoming the limitations of each method and improving the overall data quality.

Author Contributions: Conceptualization, A.P. and A.B.; methodology, P.K.; data processing software, P.K.; validation, A.P., A.B. and P.K.; formal analysis, A.P.; investigation, A.P.; resources, A.P.; data curation, A.P.; writing—original draft preparation, A.P.; writing—review and editing, A.P.; visualization, A.P.; supervision, A.P.; project administration, A.B. All authors have read and agreed to the published version of the manuscript.

Funding: This research received no external funding.

Data Availability Statement: Data are unavailable due to privacy restrictions.

Acknowledgments: We acknowledge Expert Geophysics Limited's field crews and technical support during the surveys under Mikhail Kuzmin's management and data quality control, the processors under Emily Data management, and Aamna Sirohey, a senior geophysicist, for her contributions and support in data inversions. We are grateful to Universal Copper for the permission to use their data and David Goldak (EMpulse Geophysics) for providing a TAMT digital 3D model for the comparative analysis. We sincerely thank the peer reviewers for their valuable insights and constructive feedback, which significantly enhanced the quality of this manuscript.

Conflicts of Interest: Alexander Prikhodko, Andrei Bagrianski and Petr Kuzmin are employed by Expert Geophysics Limited, Canada. The paper reflects the views of the scientists and not the companies.

References

1. Prikhodko, A.; Bagrianski, A.; Kuzmin, P.; Carpenter, A. Passive and active airborne electromagnetics—Separate and combined technical solutions and applicability. In Proceedings of the Extended Abstracts—8th International Airborne Electromagnetics Workshop, Fitzroy Island, Australia, 3–7 September 2023.
2. Prikhodko, A.; Bagrianski, A.; Kuzmin, P.; Sirohey, A. Natural field airborne electromagnetics—History of development and current exploration capabilities. *Minerals* **2022**, *12*, 583. [CrossRef]
3. Bagrianski, A.; Kuzmin, P.; Prikhodko, A. AFMAG evolution—Expanding limits. In Proceedings of the Extended Abstracts—16th SAGA Biennial Conference & Exhibition, Durban, South Africa, 6–9 October 2019.
4. Sattel, D.; Witherly, K.; Kaminski, V. A brief analysis of MobileMT data. In Proceedings of the 89th Society of Exploration Geophysicists International Exposition and Annual Meeting, SEG, San Antonio, TX, USA, 15–20 September 2019.
5. Prikhodko, A.; Bagrianski, A.; Wilson, R.; Belyakov, S.; Esimkhanova, N. Detecting and recovering critical mineral resource systems using broadband total-field airborne natural source audio frequency magnetotellurics measurements. *Geophysics* **2024**, *89*, WB13–WB23. [CrossRef]
6. Labson, V.F.; Becker, A.; Morrison, H.F.; Conti, U. Geophysical exploration with audiofrequency natural magnetic fields. *Geophysics* **1985**, *50*, 656–664. [CrossRef]
7. Bostick, F.S.; Smith, H.W. Investigation of large-scale inhomogeneities in the Earth by the magnetotelluric method. *Proc. IRE* **1962**, *50*, 2339–2346. [CrossRef]

8. Spies, B.R. Depth of investigation in electromagnetic sounding methods. *Geophysics* **1989**, *54*, 872–878. [CrossRef]
9. Key, K. MARE2DEM: A 2-D inversion code for controlled-source electromagnetic and magnetotelluric data. *Geophys. J. Int.* **2016**, *207*, 571–588. [CrossRef]
10. Rhys, D.; Sierd, E.; van der Meer, L. Geology of the Shea Creek uranium deposits—Part of an expanding uranium district in the Western Athabasca Basin. In Proceedings of the Saskatchewan Geological Survey Open House, Saskatoon, Saskatchewan, 29 November 2010; Volume 4.
11. Nimeck, G.; Koch, R. A progressive geophysical exploration strategy at the Shea Creek uranium deposit. *Lead. Edge* **2008**, *27*, 52–63. [CrossRef]
12. Geotech Ltd. ZTEM Tipper AFMAG Results over Shea Creek Unconformity Uranium Deposits. 2009. Available online: https://geotech.ca/wp-content/uploads/2015/02/012-ZTEM_Uranium_SheaCreek_Saskatchewan.pdf (accessed on 6 May 2024).
13. Jansen, J.C.; Cristall, J.A. Mineral exploration using natural EM fields. In Proceedings of the Exploration 17: Sixth Decennial International Conference on Mineral Exploration, Toronto, ON, Canada, 22–25 October 2017; Targeting 2: Mine to Camp Scale. pp. 349–377.
14. Post, R.T. *Stratigraphy and Sedimentology of the Athabasca Group in the Net Lake-Maybelle River Area, North-Eastern Alberta*; EUB/AGS Earth Sciences Report 2003-01; Alberta Energy and Utilities Board: Calgary, AB, Canada, 2004; 103p.
15. Goldak, D.; Goldak, M. Transient Magnetotellurics with Adaptive Polarization Stacking. In Proceedings of the SEG International Exposition and 71′st Annual Meeting, San Antonio, TX, USA, 9–14 September 2001; pp. 1509–1512.
16. EMpulse Geophysics Ltd. Case Histories, Shea Creek. Available online: http://www.empulse.ca/upload/documents/shea3d.pdf (accessed on 6 May 2024).
17. de Weerdt, P.; El Rassi, D.; Gagnon, D.M.; Bisaillon, C.; Liskovych, V.; Embree, K.; Stephens, B.; Shaw, S.; Gravel, A. NI 43-101 Technical Report Feasibility Study Curipamba El Domo Project, Central Ecuador. 2021. Available online: https://www.sedarplus.ca/csa-party/records/document.html?id=0f7ee7252be12656c6f52305d868c855f5b1023f1573e62980e1f20bc26b78da (accessed on 7 July 2024).
18. Vallejo, C.; Soria, F.; Tornos, F.; Naranjo, G.; Rosero, B.; Salazar, F.; Cochrane, R. Geology of El Domo deposit in central Ecuador: A VMS formed on top of an accreted margin. *Miner. Depos.* **2015**, *51*, 389–409. [CrossRef]
19. Wang, Y.; Lesher, C.M.; Lightfoot, P.C.; Pattison, E.F.; Golightly, J.P. Genesis of sublayer, footwall breccia, and associated Ni-Cu-platinum group element mineralization in the Sudbury igneous complex. *Econ. Geol.* **2022**, *117*, 1791–1807. [CrossRef]
20. Balch, S.J. The geophysical signatures of platinum-group element deposits. In *Exploration for Platinum-Group Elements Deposits*; Mungall, G.E., Ed.; Mineralogical Association of Canada Short Course Series; Mineralogical Association of Canada: Québec City, QC, Canada, 2005; Volume 35, pp. 275–285.
21. Olaniyan, O.; Smith, R.S.; Morris, B. Qualitative geophysical interpretation of the Sudbury Structure. *Interpretation* **2013**, *1*, T25–T43. [CrossRef]
22. Ashton, J.; Robb, W. *Technical Report on the Poplar Deposit, Omineca Mining Division*; Universal Copper Ltd.: Vancouver, BC, Canada, 2021.
23. Woodall, R.; Travis, G.A. The Kambalda nickel deposits, Western Australia. In Proceedings of the 9th Commonwealth Mining Metallurgy Congress, London Institute of Mining Metallurgy, London, UK, 29 May 29–5 June 1969; p. 26.
24. Gaspericova, E.; Morrison, H.F. Mapping of induced polarization using natural fields. *Geophysics* **2001**, *66*, 137–147. [CrossRef]
25. Hermance, J.F.; Thayer, R.E. The telluric-magnetotelluric method. *Geophysics* **1975**, *40*, 664–668. [CrossRef]
26. Zhdanov, M.S. Electromagnetic geophysics: Notes from the past and the road ahead. *Geophysics* **2010**, *75*, 75A49–75A66. [CrossRef]